

Supporting Information

Ni-perovskite interaction and its structural and catalytic consequences in methane steam reforming and methanation reactions

Ramona Thalinger¹, Martin Gocyla², Marc Heggen², Rafal Dunin-Borkowski², Matthias Grünbacher¹, M. Stöger-Pollach³, Daniela Schmidmair⁴, Bernhard Klötzer¹, Simon Penner^{1*}

¹*Institute of Physical Chemistry, University of Innsbruck, Innrain 80-82, A-6020 Innsbruck,
Austria*

²*Ernst Ruska-Centrum und Peter Grünberg Institut, Forschungszentrum Jülich GmbH, 52425
Jülich, Germany*

³*University Service Centre for Transmission Electron Microscopy (USTEM), Vienna,
University of Technology, Wiedner Hauptstrasse 8-10/052, A-1040, Vienna, Austria*

⁴*Institute of Mineralogy and Petrography, University of Innsbruck, Innrain 52d, A-6020
Innsbruck, Austria*

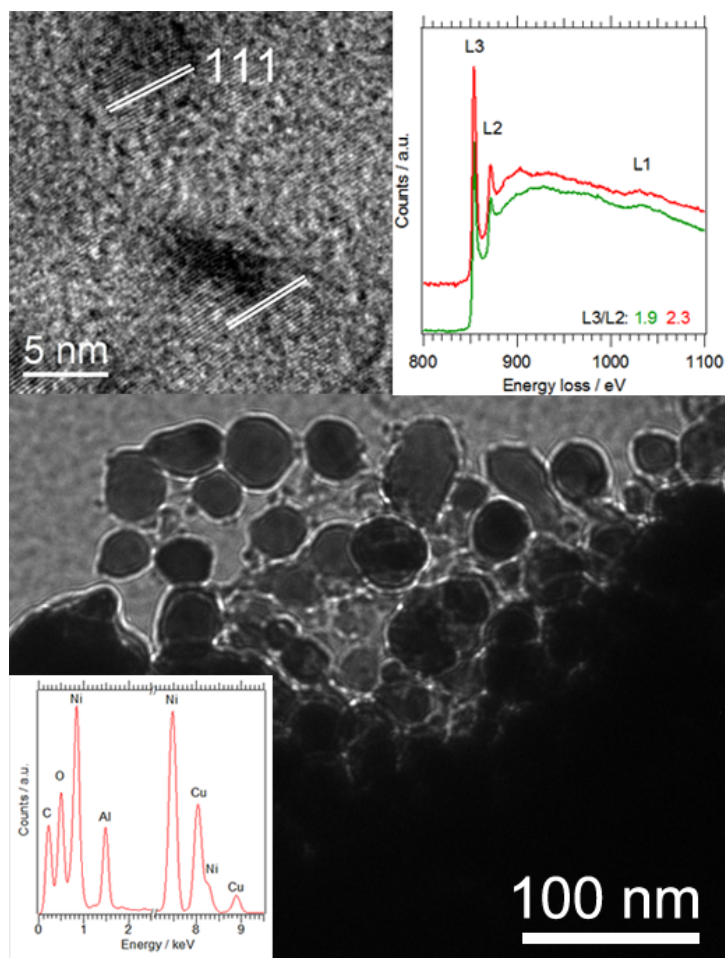


Figure S1: Overview TEM image of the Ni-Al₂O₃ reference catalyst in the as-prepared state (main panel), high-resolution image of two Ni particles with (111) lattice fringes (top left). Top right: EEL spectra of different spots on the Ni-Al₂O₃ catalyst. Bottom left: EDX spectrum of the Ni-Al₂O₃ material.

For the sake of clarity, the reference catalyst is – as in the main paper - in the following referred to as “Ni-Al₂O₃”, although the precursor material is Ni-AlOOH (boehmite). The main panel shows an overview TEM image of a single support grain with an array of large NiO particles of 20 to 70 nm. The EDX spectrum in the lower left corner reveals that indeed the catalyst is only composed of Ni, O and Al - apart from carbon and Cu arising from the Cu grid covered with a perforated carbon film. In addition, both the high-resolution image (with corresponding (111) lattice planes of cubic NiO; upper left inset) and the EEL spectra (upper right inset) reveal the predominant presence of NiO. Specifically, EEL spectra taken from

various Ni particles indicate a slightly different Ni L₃/L₂ ratio, indicative of Ni in different oxidation states. The higher the ratio, the more oxidized the Ni particles are. As the intensity ratios slightly vary (from Ni L₃/L₂ 1.9 to 2.3) we might infer the simultaneous presence of Ni and NiO particles.

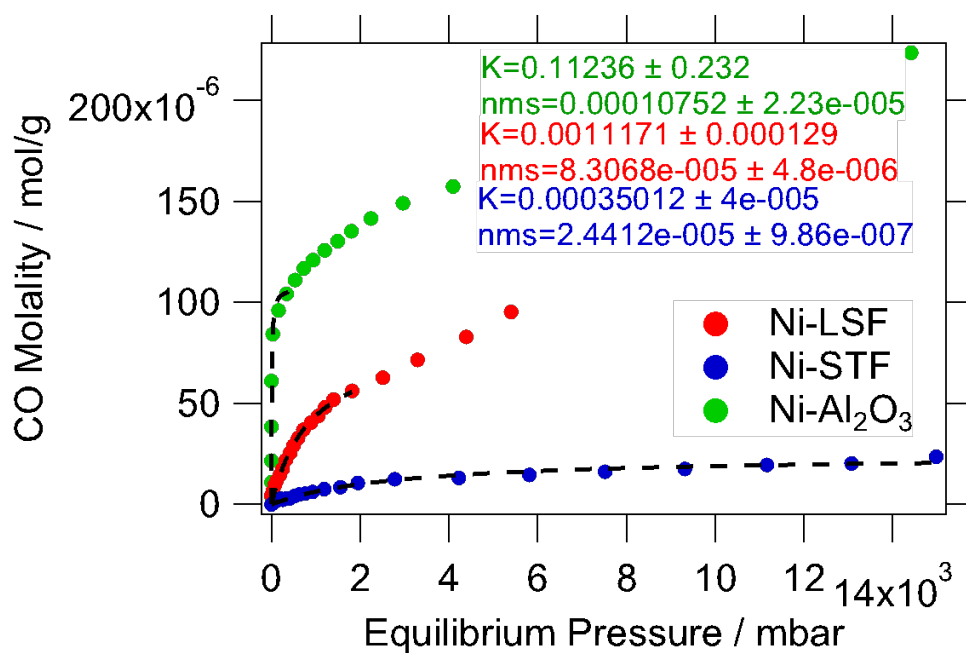


Figure S2: CO adsorption measurements on Ni-LSF (red), Ni-STF (blue) and Ni-Al₂O₃ (green) at room temperature. The adsorbed amount of CO normalized to the catalyst mass is shown versus the CO equilibrium pressure. A spillover effect can be clearly seen on all three samples.

To indirectly validate the TEM measurements, the calculated accessible Ni sites, and hence the apparent activation energies and the resulting TOF values have been also determined by additional hydrogen and CO chemisorption measurements. Before these measurements, the catalysts were oxidized (400 °C, O₂, 1 bar) and pre-reduced (600 °C, H₂, 1 h). Hydrogen was subsequently removed by temperature-programmed desorption up to 600 °C. While the hydrogen chemisorption measurements are too affected by H₂ adsorption as a side reaction blurring the adsorption on the metal surface, the corresponding CO adsorption experiments (although the same limitation of perovskite reduction by CO in principle applies) indeed

directly validate the TEM calculations. Table 1 summarizes these data. Experimentally, CO has been stepwise added at room temperature under static conditions until quasi-saturation has been observed. The corresponding data are shown in the SI. Note, as stated above, spill-over effects impede the clear saturation. To circumvent these problems, Langmuir fits have been applied and used for calculation the amount of adsorbed CO, the number of active sites and the TOF values. The accuracy of the analysis is revealed by the good agreement between TEM and adsorption studies. The apparent activation energies for the CO₂ methanation reaction are calculated on the basis of an Arrhenius fit to the TOF vs. reaction temperature graphs, both derived from the TEM results and the CO chemisorption measurements and for all three catalysts. The fits are highlighted in the SI, the derived data jointly shown in Table 1, main paper.

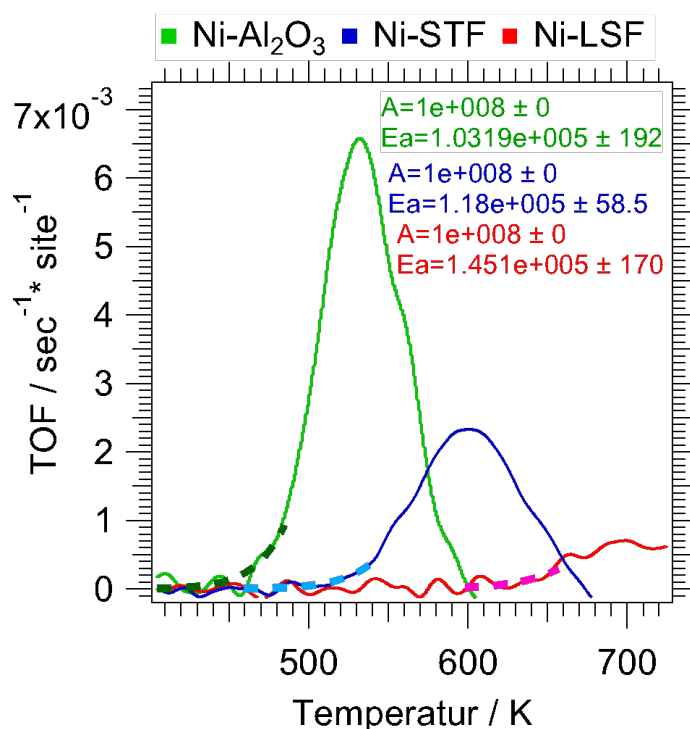


Figure S3: TOF values for the CO₂ methanation reaction calculated with number of Ni sites as estimated from the TEM particle size distribution for Ni-Al₂O₃ (green), Ni-STF (red) and Ni-LSF (blue) with according Arrhenius fits to the initial reaction rate (dashed lines).

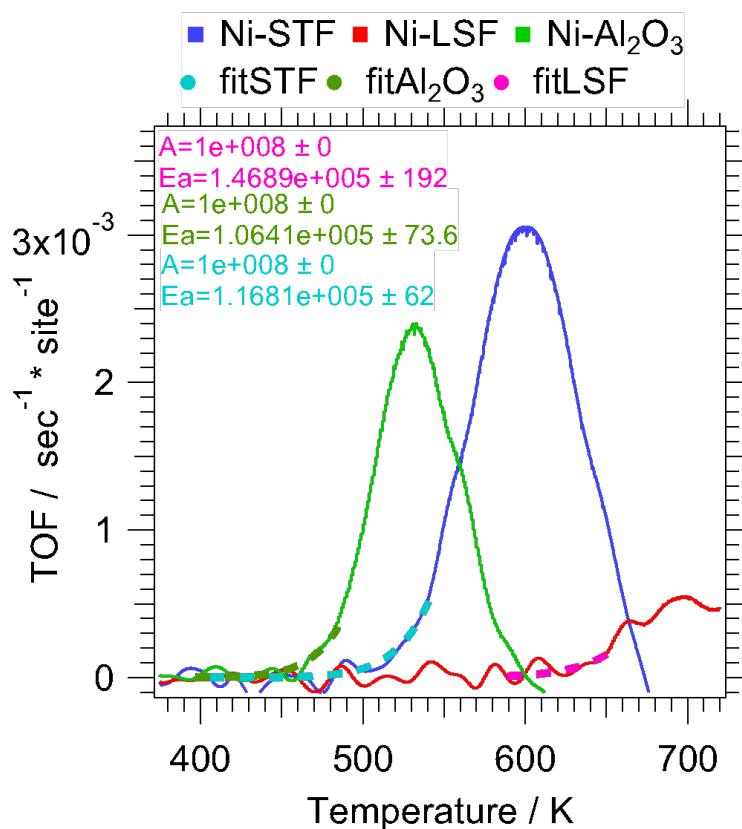


Figure S4: TOF values for the CO₂ methanation reaction calculated with number of Ni sites as estimated from the CO adsorption measurements for Ni-Al₂O₃ (green), Ni-STF (red) and Ni-LSF (blue) with according Arrhenius fits to the initial reaction rate (dashed lines).

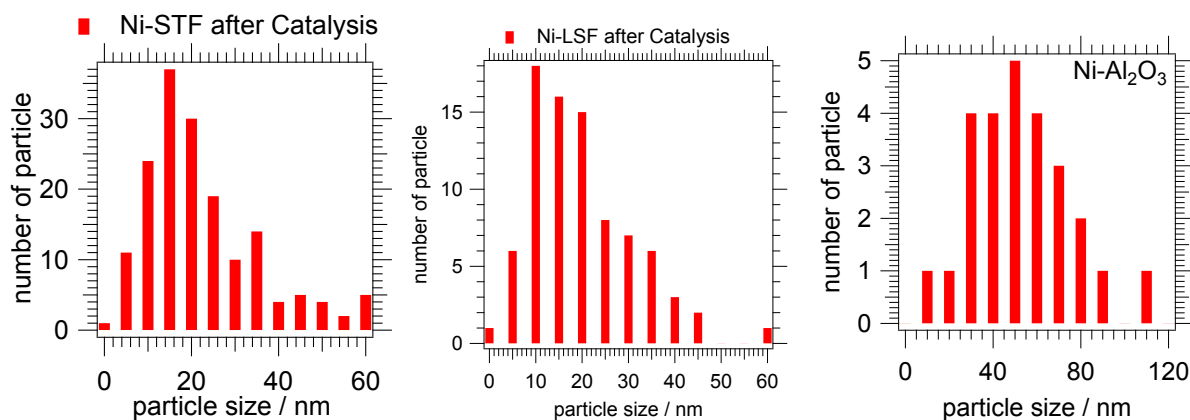


Figure S5: Particle size distribution of Ni-STF (left), Ni-LSF (middle) and Ni-Al₂O₃ (right) after the CO₂ methanation reaction.

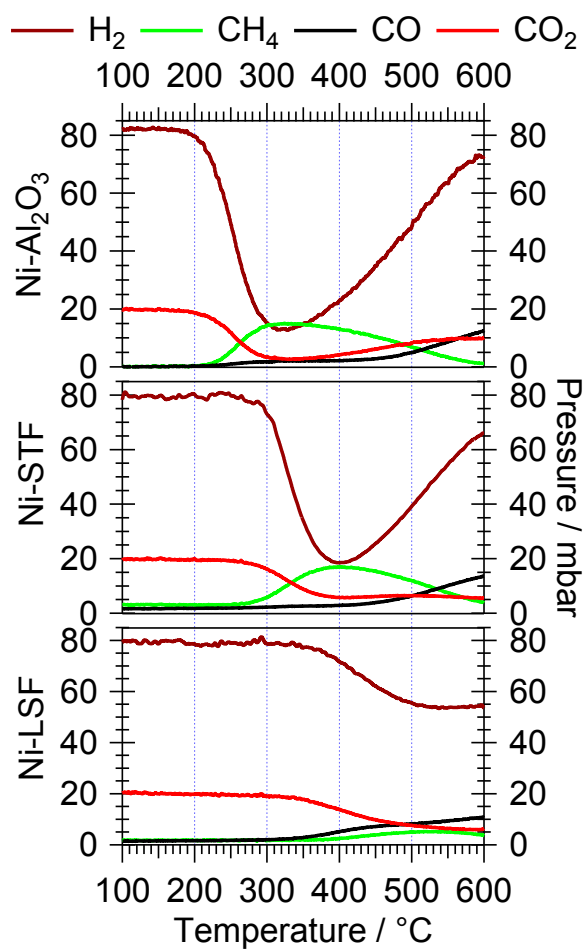


Figure S6: CO₂ methanation reaction from CO₂ ($CO_2 + 4H_2 \rightarrow CH_4 + 2H_2O$) on the Ni-Al₂O₃ reference catalyst (upper panel) in comparison to the same reaction on Ni-STF (middle panel) and Ni-LSF (lower panel). Reaction conditions: 20 mbar CO₂, 80 mbar H₂ and 25 mbar H₂O, 10 mbar Ar, He added to 1 bar total pressure. Heating rate: 5 °C min⁻¹.

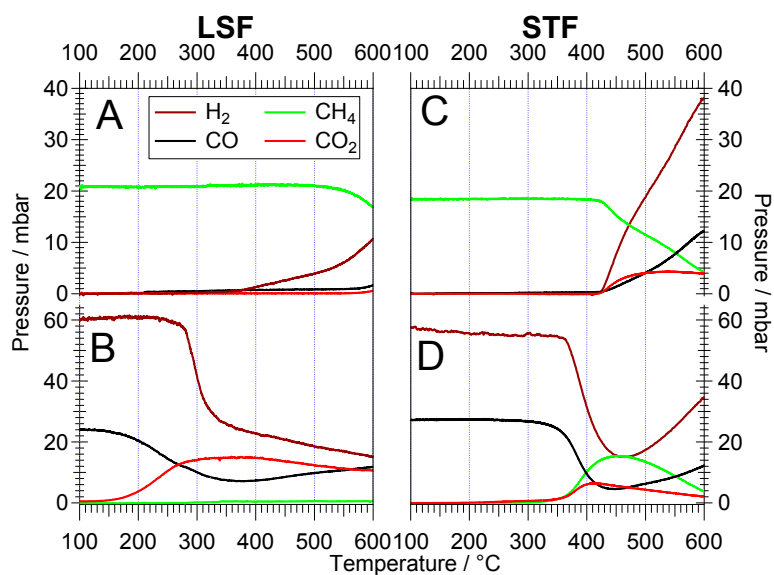


Figure S7: Methane steam reforming $CH_4 + xH_2O \rightarrow CO_x + (2 + x)H_2$ (panel A and C; 25 mbar H₂O and 25 mbar CH₄), as well as CO methanation ($CO + 3H_2 \rightarrow CH_4 + H_2O$; panels B and D; 20 mbar CO, 60 mbar H₂) on Ni-LSF (panels A-B) and Ni-STF (panels C-D). 10 mbar Ar added for correction of gas withdrawal, He added to 1 bar total pressure. Heating rate: 5 °C min⁻¹.

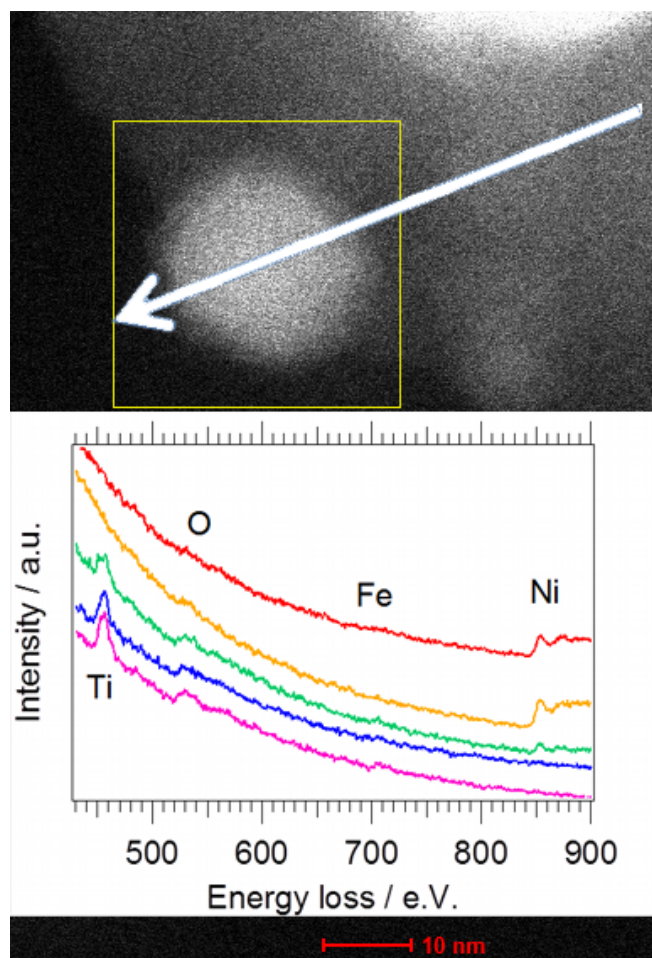


Figure S8: EELS line scans on Ni-STF after static reduction at 600 °C to exemplarily prove that at no point Fe particle exsolution has been found.